Site Specific X-ray Anomalous Dispersion of the Geometrically Frustrated Kagomé Magnet, Herbertsmithite, ZnCu$_3$(OH)$_6$Cl$_2$

Danna E. Freedman,[†] Tianheng H. Han,[‡] Andrea Prodi,[‡] Peter Müller,[†] Qing-Zhen Huang,[§] Yu-Sheng Chen,[||] Samuel M. Webb,[⊥] Young S. Lee,[‡] Tyrel M. McQueen,[†,#] and Daniel G. Nocera*,[†]

Department of Chemistry, 6-335, Massachusetts Institute of Technology, Cambridge, Massachusetts 02139, Department of Physics, Massachusetts Institute of Technology, Cambridge, Massachusetts 02139, National Institute of Standards and Technology, Gaithersburg, Maryland 20899, Advanced Photon Source, Argonne, Illinois 60439, and SSRL, SLAC National Accelerator Laboratory, Menlo Park, California 94025

Received August 5, 2010; E-mail: nocera@mit.edu

Abstract: Structural characterization, exploiting X-ray scattering differences at elemental absorption edges, is developed to quantitatively determine crystallographic site-specific metal disorder. We apply this technique to the problem of Zn−Cu chemical disorder in ZnCu$_3$(OH)$_6$Cl$_2$. This geometrically frustrated kagomé antiferromagnet is one of the best candidates for a spin-liquid ground state, but chemical disorder has been suggested as a mundane explanation for its magnetic properties. Using anomalous scattering at the Zn and Cu edges, we determine that there is no Zn occupation of the intralayer Cu sites within the kagomé layer; however there is Cu present on the Zn intersite, leading to a structural formula of (Zn$_{0.85}$Cu$_{0.15}$)-Cu$_3$(OH)$_6$Cl$_2$. The lack of Zn mixing onto the kagomé lattice sites lends support to the idea that the electronic ground state in ZnCu$_3$(OH)$_6$Cl$_2$ and its relatives is nontrivial.

Introduction

Materials whose electrons exhibit nontrivial, "emergent" quantum states have been pursued for more than 50 years.[1−3] One of the most sought of these is the resonating valence bond (RVB) "spin-liquid" state, which has been proposed as the ground state of both undoped copper oxide superconductors and low dimensional geometrically frustrated antiferromagnets.[4,5] Currently, the most promising candidates possessing an RVB state are the layered compounds, Zn$_x$Cu$_{4-x}$(OH)$_6$Cl$_2$ and Mg$_x$Cu$_{4-x}$(OH)$_6$Cl$_2$.[6−8] The geometric frustration imposed by the two-dimensional (2D) $S = 1/2$ antiferromagnet lattice of these compounds can suppress classical magnetic long-range order (LRO) and thus engender novel spin liquid properties.[3,7,9−11] However, a challenge in establishing these materials as spin liquids rests in authenticating that the suppressed LRO behavior is in fact due to a nontrivial electronic state, rather than more mundane effects such as chemical disorder. In the case of the "$x = 1$" end member of Zn$_x$Cu$_{4-x}$(OH)$_6$Cl$_2$, chemical disorder between Zn^{2+} and Cu^{2+} has previously been suggested[9,12−16] and could explain the observed physical properties without invoking the presence of an RVB state.[17] Here we appropriate the technique of anomalous X-ray diffraction, commonly used in protein crystallography for structure phasing,[18,19] to quantitatively determine the level of Zn−Cu mixing in ZnCu$_3$-(OH)$_6$Cl$_2$. We find that, contrary to previous reports of similar materials,[9,12−16] there is very little mixing of Zn^{2+} onto the Cu^{2+} sites of the kagomé planes and that the compound previously

† Department of Chemistry, 6-335, Massachusetts Institute of Technology.
‡ Department of Physics, Massachusetts Institute of Technology.
§ National Institute of Standards and Technology.
|| Advanced Photon Source.
⊥ SLAC National Accelerator Laboratory.
Present Address: Department of Chemistry and Department of Physics and Astronomy, The Johns Hopkins University, Baltimore, MD 21218.

(1) Balents, L. *Nature* **2010**, *464*, 199–208.
(2) Leggett, A. J. *Nat. Phys.* **2006**, *2*, 134–136.
(3) Moessner, R.; Ramirez, A. R. *Phys. Today* **2006**, *59*, 24–29.
(4) Anderson, P. W. *Science* **1987**, *235*, 1196–1198.
(5) Anderson, P. W. *Mater. Res. Bull.* **1973**, *8*, 153–160.
(6) Shores, M. P.; Nytko, E. A.; Bartlett, B. M.; Nocera, D. G. *J. Am. Chem. Soc.* **2005**, *127*, 13462–13463.
(7) Helton, J. S.; Matan, K.; Shores, M. P.; Nytko, E. A.; Bartlett, B. M.; Yoshida, Y.; Takano, Y.; Suslov, A.; Qiu, Y.; Chung, J. H.; Nocera, D. G.; Lee, Y. S. *Phys. Rev. Lett.* **2007**, *98*, 107204/1–4.
(8) Chu, S.; McQueen, T. M.; Chisnell, R.; Freedman, D. E.; Müller, P.; Lee, Y. S.; Nocera, D. G. *J. Am. Chem. Soc.* **2010**, *132*, 5570–5571.
(9) Imai, T.; Nytko, E. A.; Bartlett, B. M.; Shores, M. P.; Nocera, D. G. *Phys. Rev. Lett.* **2008**, *100*, 077203/1−5.
(10) Lee, P. A. *Rep. Prog. Phys.* **2008**, *71*, 012501.
(11) Ramirez, A. P. *Annu. Rev. Mater. Sci.* **1994**, *24*, 53–80.
(12) Lee, S. H.; Kikuchi, H.; Qiu, Y.; Lake, B.; Huang, Q.; Habicht, K.; Kiefer, K. *Nat. Mater.* **2007**, *6*, 853–857.
(13) de Vries, M. A.; Kamenev, K. V.; Kockelmann, W. A.; Sanchez-Benitez, J.; Harrison, A. *Phys. Rev. Lett.* **2008**, *100*, 157205/1–4.
(14) Bert, F.; Olariu, A.; Zorko, A.; Mendels, P.; Trombe, J. C.; Duc, F.; de Vries, M. A.; Harrison, A.; Hillier, A. D.; Lord, J.; Amato, A.; Baines, C. *Phys. Rev. B* **2007**, *76*, 132411/1–4.
(15) Chitra, R.; Rozenberg, M. J. *Phys. Rev. B* **2008**, *77*, 052407/1–4.
(16) Olariu, A.; Mendels, P.; Bert, F.; Duc, F.; Trombe, J. C.; de Vries, M. A.; Harrison, A. *Phys. Rev. Lett.* **2008**, *100*, 087202/1−4.
(17) Singh, R. R. P. *Phys. Rev. Lett.* **2010**, *104*, 177203/1−4.
(18) Guss, J. M.; Merritt, E. A.; Phizackerley, R. P.; Hedman, B.; Murata, M.; Hodgson, K. O.; Freeman, H. C. *Science* **1988**, *241*, 806–811.
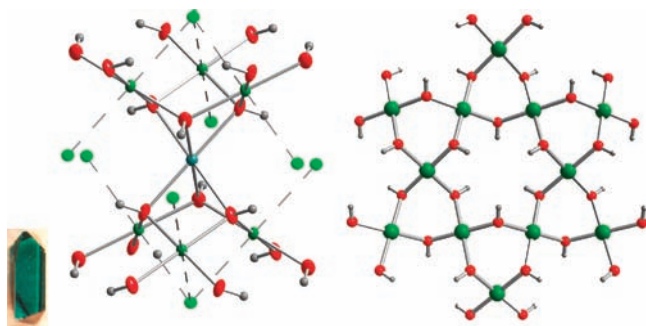(19) Ealick, S. E. *Chem. Biol.* **2000**, *4*, 495–499.

Figure 1. Crystal structure of herbertsmithite obtained with 0.41×10^{-10} m wavelength data. Blue, green, bright green, red, and gray spheres represent Zn, Cu, Cl, O, and H atoms, respectively. (a) Local coordination environment of the intersite is highlighted in a projection perpendicular to the *c*-axis. Thermal ellipsoids are drawn at the 70% probability level. (b) The geometry of the kagomé layer is highlighted, in a projection perpendicular to the *c*-axis. All atoms outside the kagomé plane have been removed for clarity. (c) Photograph of a crystal from the batch used for these data. Selected interatomic distances (Å) and angles (deg): Zn−O, 2.1073(5); Cu−O, 1.9821(3); Cu−Cl, 2.7676(2); Zn···Cu, 3.0560; O−Zn−O, 76.57(2), 103.43(2), 180.00(2); O−Cu−O, 81.7(3), 98.3(3), 180.0; O−Cu−Cl, 82.41(3), 97.421(13); Cl−Cu−Cl, 180.0; Cu−O−Cu, 118.66(3); Cu−O−Zn, 96.662(17).

identified as $ZnCu_3(OH)_6Cl_2$ is actually $(Zn_{0.85}Cu_{0.15})Cu_3(OH)_6Cl_2$. These results imply that chemical disorder within the 2-D kagomé network is not the underlying cause of the unusual magnetic properties of $ZnCu_3(OH)_6Cl_2$ and lend support to the idea that the electronic ground state of $ZnCu_3(OH)_6Cl_2$ and its relatives is nontrivial.

The structure of $ZnCu_3(OH)_6Cl_2$ shown in Figure 1 consists of kagomé planes of hydroxide bridged $S = 1/2$ Cu^{2+} centers with Cu−O−Cu bond angles of 119°. The Cu^{2+} ions reside in a tetragonally elongated O_4Cl_2 chemical environment, with equatorial Cu−O distances of 1.98 Å and apical Cu−Cl bond lengths of 2.77 Å. The kagomé layers are separated by $[Zn(OH)_6]^{4-}$ octahedral units connected to the kagomé layers through the hydroxide ligands, with Zn−O−Cu bond angles of 96.7°. Each Zn^{2+} ion resides on a $-3m$ site leading to six equivalent Zn−O distances of 2.10 Å. The nontrivial difference between the slightly trigonally compressed octahedral ligand field of the Zn^{2+} ions and the significantly Jahn−Teller elongated environment of the Cu^{2+} ions is expected to engender a strong site preference for Cu^{2+} in the kagomé plane and Zn^{2+} in the intersite positions. Despite the expected site preference, $ZnCu_3(OH)_6Cl_2$ is the end member of the solid solution, $Zn_xCu_{4-x}(OH)_6Cl_2$, in which the intersite cation varies in composition from $x = 1$ to $x = 0$.[6] The stability of these intermediate phases suggests the potential for site disorder, as has been previously suggested.[9,12−16] Dc magnetic susceptibility data collected for the $x = 0$ compound display a sharp ferromagnetic ordering transition at 6.5 K, stemming from weak interlayer ferromagnetic coupling between the Cu^{2+} cations within the kagomé plane and the Cu^{2+} cations on the intersite positions. Indeed, such weak ferromagnetic superexchange, as observed here, is predicted by the Goodenough−Kanamori rules for an M−O−M bond angle of 96.7°.[20,21] As the occupancy of intersite Cu^{2+} ions is reduced, the magnetic ordering transition softens, eventually disappearing for materials with the nominal composition of $ZnCu_3(OH)_6Cl_2$. Fits of the Curie−Weiss law to the inverse susceptibility indicate strong antiferromagnetic

coupling, on the order of $J \approx -200$ K, as predicted by the Goodenough−Kanamori rules for a bond angle of 119°.[20,21] The absence of a magnetic ordering transition to 50 mK in samples of $ZnCu_3(OH)_6Cl_2$ is strongly indicative of an RVB ground state.[7] Alternatively, Zn impurities on the kagomé lattice or Cu impurities on the intersite could lead to either a spin liquid or, as has recently been proposed, a valence bond glass state.[17] Either of these states could also account for the unusual magnetic and physical properties displayed by $ZnCu_3(OH)_6Cl_2$. Recently, on the basis of single crystal X-ray and neutron powder diffraction (NPD) data, it has been argued that, in samples previously categorized as pure $ZnCu_3(OH)_6Cl_2$, there is significant population of Zn^{2+} on the kagomé lattice, and correspondingly, a large percent of Cu^{2+} on the intersite.[12,13] However, the X-ray scattering factors of Zn and Cu are virtually identical, preventing precise discrimination of Zn and Cu by single crystal X-ray diffraction. The neutron scattering lengths do differ more, by ~30%, but the powder measurement significantly constrains the number of independent reflections, limiting the precision to which Zn and Cu can be differentiated.

To clarify this debate surrounding $ZnCu_3(OH)_6Cl_2$ and to understand its unusual physics, accurate structural characterization of this compound is needed. Toward this end, a more precise experimental technique to differentiate between Zn and Cu on different crystallographic sites was sought. We herein use X-ray anomalous scattering data not only to identify atom types on individual crystallographic sites but also to quantify the level of Zn and Cu present at each site. A paucity of reports of the quantification of disorder by anomalous diffraction exists within the literature,[22−29] with most examples restricted to powder diffraction. To the best of our knowledge, all previous examples of anomalous scattering for disorder quantification have involved either noncentrosymmetric crystal structures or centrosymmetric ones with special reflection conditions for the crystallographic sites of concern. Data analysis in these specific cases is trivial, but a fully generalized technique has not been forthcoming. Here we demonstrate an improved methodology that allows us to quantify the degree of Zn−Cu disorder in herbertsmithite. We find that, contrary to previous reports,[12−16] while there is Cu^{2+} population on the interlayer sites occupied by Zn^{2+}, there is negligible mixing of Zn^{2+} onto the Cu^{2+} sites of the kagomé intralayer. The compound's composition is determined to be $(Zn_{0.85}Cu_{0.15})Cu_3(OH)_6Cl_2$. The validity of the anomalous scattering X-ray diffraction experiments are confirmed by a combination of EXAFS measurements and low temperature NPD data.

Experimental Section

Preparation of Single Crystals of $ZnCu_3(OH)_6Cl_2$. A quartz tube (6 mm ID, 13 mm OD) was charged with CuO (0.235 g, 2.95

(20) Goodenough, J. B. *J. Phys. Chem. Sol.* **1958**, *6*, 287−297.
(21) Kanamori, J. *J. Phys. Chem. Sol.* **1959**, *10*, 87−98.

(22) Wulf, R. *Acta Crystallogr.* **1990**, *A46*, 681−688.
(23) Okita, A.; Saito, F.; Sasaki, S.; Toyoda, T.; Koinuma, H. *Jpn. J. Appl. Phys.* **1998**, *37*, 3441−3445.
(24) Bernard, F.; Lorimier, J.; Nivoix, V.; Millot, N.; Perriat, P.; Gillot, B.; Berar, J. F.; Niepce, J. C. *J. Solid State* **1998**, *141*, 105−113.
(25) Matsumura, T.; Okuyama, D.; Niioka, S.; Ishida, H.; Satoh, T.; Murakami, Y.; Toyosaki, H.; Yamada, Y.; Fukumura, T.; Kawasaki, M. *Phys. Rev. B* **2007**, *76*, 115320.
(26) Zhang, Y.; Wilkinson, A. P.; Nolas, G. S.; Leea, P. L.; Hodges, J. P. *J. Appl. Crystallogr.* **2003**, *36*, 1182−1189.
(27) Zhang, Y.; Wilkinson, A. P.; Lee, P. L.; Shastri, S. D.; Shu, D.; Chung, D.-Y.; Kanatzidis, M. G. *J. Appl. Crystallogr.* **2005**, *38*, 433−441.
(28) Caticha-Ellis, S. *Acta Crystallogr.* **1962**, *15*, 863−865.
(29) Battle, P. D.; Blundell, S. J.; Coldea, A. I.; Cussen, E. J.; Rosseinsky, M. J.; Singleton, J.; Springa, L. E.; Ventea, J. F. *J. Mater. Chem.* **2001**, *11*, 160−167.

mmol), $ZnCl_2$ (2.015 g, 14.82 mmol), and H_2O (4.5 mL). The tube was then purged with air by a mechanical pump and sealed with a hydrogen flame. The sample was placed into an oven at 185 °C for 2 days, at which point a green-blue $Zn_xCu_{4-x}(OH)_6Cl_2$ micro-crystalline powder formed. Millimeter-sized single crystals were grown by the following recrystallization process: Placing the tubing vertically at room temperature, the powder was condensed into one end. Then the tube was carefully loaded horizontally into a three zone furnace, and a temperature gradient was set which slowly transports the powder to the other end of the tube for crystallization. The temperature was slowly increased until the powder source material reached 180 °C. The sample was left undisturbed until large crystals suitable for X-ray diffraction formed at the cold end. The temperature gradient at the cool end of the tube, where the crystals nucleated and grew, was measured to be around 1 °C/cm. ICP-AES analysis found a Zn/Cu ratio of 0.97:3.03, within the standard 5% instrument error of 1:3.

Neutron Powder Diffraction. Deuterated powder samples of herbertsmithite for NPD were prepared as previously reported, with the substitution of H_2O with D_2O. High resolution neutron powder diffraction (NPD) data were collected using the BT-2 (now BT-1) high-resolution powder diffractometer at the NIST Center for Neutron Research, employing a Cu(311) monochromator to produce a monochromatic neutron beam of wavelength 1.5403 Å. Collima-tors with horizontal divergences of 15′, 20′, and 7′ full width at half-maximum were used before and after the monochromator, and after the sample, respectively. The intensities were measured in steps of 0.05° in the 2θ range 3°−168°. Data was collected at room temperature and 11 K. The structure analysis was performed using the program GSAS with EXPGUI.[30,31] The neutron scattering amplitudes used in the refinements were 0.568, 0.7718, 0.5803, 0.6671, and 0.9577 (× 10^{-12} cm) for Zn, Cu, O, D, and Cl, respectively. The degree of deuteration was allowed to vary and found to be 99(1)% in all refinements. ICP-AES analysis found a Zn/Cu ratio of 1.00:3.00 ± 0.04, within the standard 5% machine error of 1:3.

EXAFS. The EXAFS spectra of the K-edges of Cu and Zn were collected with a double crystal Si(111) monochromator on beamline X18B of the National Synchrotron Light Source at Brookhaven National Laboratory. All samples were measured in transmission mode with powdered samples affixed to Kapton tape. The energy was calibrated with Cu or Zn metal foils for the Cu and Zn edges at 8979 and 9659 eV respectively. EXAFS data were processed and analyzed with SIXPACK[32] which uses the IFEFFIT[33] data analysis engine. All theoretical phases and amplitudes for EXAFS fits were calculated with FEFF7.[34]

Anomalous Scattering. A crystal suitable for X-ray diffraction was mounted on a glass fiber affixed to a copper pin. Data were collected at ChemMatCARS at the Advanced Photon Source at Argonne National Laboratory (CARS Center for Advanced Radia-tion Sources). The data set was collected at 95 K using a diamond(111) crystal monochromator and a Bruker CCD detector with 1 s counting per frame. The incident X-ray wavelengths used were as follows: two preceding the Cu edge: 1.41228×10^{-10} m, 1.3964×10^{-10} m; the Cu edge at 1.3804×10^{-10} m; three between the two edges, 1.3412×10^{-10} m, 1.31075×10^{-10} m, 1.29704×10^{-10} m; the Zn edge at 1.28361×10^{-10} m; and finally one point after the Zn edges, 1.27046×10^{-10} m. A data set was also collected at 0.41382×10^{-10} m, far from all element absorption edges, for overall structure determination. Quantification was accomplished through an error minimization routine which was written in C to

find the best f' and f'' values while minimizing $wR2$. Atomic coordinates and thermal displacements were calculated from data collected at 0.41×10^{-10} m and determined to be within error of the literature structure. Five parameters were refined, f' and f'' for each of the two sites and an overall scale factor. Uncertainties were estimated from the shape of the minimum of $wR2$ and were ~1%. Values of f' and f'' calculated for each crystallographic site were used to determine the degree of Zn−Cu mixing on each site. The quantity of Cu on the intersite was determined by comparing the values of f' for this site to a smooth curve, generated with the value of f' congruent with Zn = 1, −2.84. The best fit value of Cu f' on the intersite site at the Cu edge is −3.51. Thus the approximate Cu occupation of the site is a value f such that $(1 - f)^* - 2.84 + f^* - 7.9 = -3.51$, or $f_I = 0.13 = 13\%$. The same approach on the absorption correction data gives $f_I = 17\%$. Thus the Cu occupation of the intersite is estimated to be 15%. A similar approach was used for the kagomé site around the Zn edge. With no absorption correction, there is no deviation from a smooth curve and thus the percent of Zn on the kagomé site is zero. After absorption correction, $f_K = 2\%$. Thus the Zn occupation of the Cu site is estimated to be at most 1%. This leads to an overall Zn/Cu ratio of 0.88:3.12 (= 0.28:1). The complete source code for the program, including compilation and operating instructions, is available online at the time of publication at http://occamy.chemistry.jhu.edu/anomalous.

Results and Discussion

Crystals suitable for single crystal X-ray diffraction were grown by recrystallization of the microcrystalline product. X-ray anomalous scattering measurements of these crystals were acquired at beamline 15-ID-C at the Advanced Photon Source (APS) at Argonne National Laboratory. To permit independent quantification of Zn and Cu occupancies, and to account for any changes in anomalous scattering factors due to crystal effects, data were collected near the K-edges of Cu and Zn at a spectrum of wavelengths spanning both absorption edges. For overall structure determination, a data set was also collected far from all absorption edges (see Experimental Section).

In a modification of the literature methods,[22] Fourier differ-ence maps were calculated between the structure and the reflection data at each wavelength to judge qualitatively the level of site mixing. At an absorption edge, electron density holes were expected at the atomic coordinates of the anomalous scatterer with electron density peaks at all other atomic coordinates. This effect can be attributed to a quantity of the photons that are scattered from the anomalous scatterer and do not meet the expected diffraction conditions, leading to an apparent decrease in the size of the electron cloud of the anomalous scatterer. In order to extract these data, difference maps were obtained in the kagomé plane at $z = 0.16667$ and at the intersite plane of $z = 0$.

Fourier difference maps for data obtained at the Cu edge (Figure 2a,b) display deep electron density holes of -2 e/Å³ at the Cu coordinates on the kagomé plane, corresponding to 7% of the total electron density of the Cu atom. On the intersite slice, peaks of 2 e/Å³ appear at the Zn coordinates, with no additional electron density in the plane. At the Zn edge (Figure 2c,d), the effect is reversed with the Fourier difference map displaying deep holes of -3 e/Å³ at the intersite, corresponding to 10% of the total electron density of Zn. On the kagomé plane, peaks of 3 e/Å³ appear at the Cu atomic coordinates. Data acquired at the Cu edge employed a wavelength that slightly preceded the absorption edge; thus both the holes and peaks are smaller than those for the data collected at the Zn edge. This data provide a qualitative distinction between Cu and Zn

(30) Toby, B. H. *J. Appl. Crystallogr.* **2001**, *34*, 210–213.
(31) Larson A. C.; Von Dreele R. B. *General Structure Analysis System (GSAS) Los Alamos National Laboratory Report LAUR 86-748* (http://www.ccp14.ac.uk/ccp/ccp14/ftp-mirror/gsas/public/ gsas/manual/GSASManual.pdf, 2000).
(32) Webb, S. M. *Phys. Scr.* **2005**, *T115*, 1011–1014.
(33) Newville, M. *J. Synch. Rad.* **2001**, *8*, 332–324.
(34) Rehr, J. J.; Zabinsky, S. I.; Albers, R. C. *Phys. Rev. Lett.* **1992**, *69*, 3397–3340.
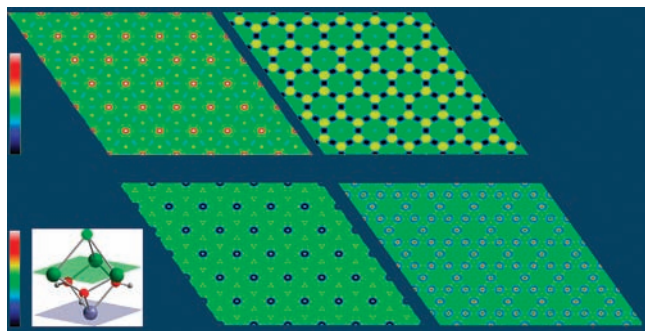
Figure 2. Fourier difference maps were calculated between the structure and the reflection data. Top: Difference maps at the Cu K-edge on a linear scale of 2 to -2 e/Å^3, shown at the left. Bottom: Difference maps at the Zn K-edge on a linear scale of 3 to -3 e/Å^3, shown at the left. Maps on the left were calculated in the intersite containing plane $z = 0$, and maps on the right were calculated at the kagomé layer containing plane $z = 0.16667$. Corner: Portion of the crystal structure demonstrating the planes used to calculate the difference maps; purple represents $z = 0$, and green represents $z = 0.1667$.
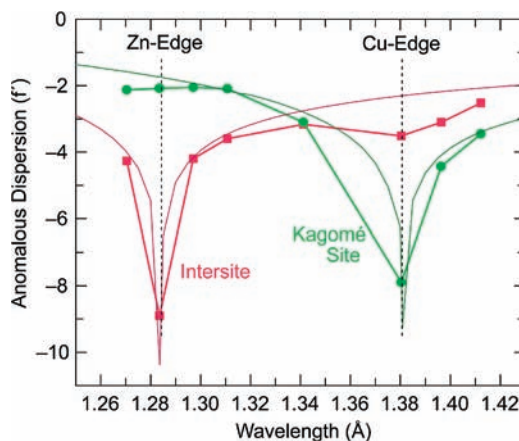

Figure 3. Anomalous dispersion calculated at each wavelength of data collection. Values obtained for the kagomé site are plotted as bright green circles, while values obtained for the intersite are plotted as red squares. The lines connecting them serve as a guide for the eyes. Also shown are the calculated f' edge values for the Zn K-edge (dark red) and the calculated values for the Cu K-edge (dark green). The absorption edges of both Zn and Cu have been delineated by a dotted line.

in the structure and suggest, to a first approximation, that there is no Zn–Cu mixing. Initially it was hoped that quantification could be accomplished by scaling small holes in the Fourier difference map at partially occupied sites; however site mixing contributions could not be placed on an absolute scale, preventing the implementation of this method.

Instead, data were quantified by least-squares refinement of the structure model and the reflection data, using the structure factor equation, with the real (f') and imaginary (f'') components to the scattering factor (eq 1) as parameters. A standard least-squares minimization algorithm was used to find the minimum in $wR2(F^2)$.

$$F(h, k, l) = \sum_{j=1}^{\text{atoms}} (f^0 + f' + i \cdot f'') \exp(2\pi \cdot i(hx_{(j)} + ky_{(j)} + lz_{(j)}))$$

(1)

This approach mimics small molecule crystal refinement protocols, in which the structure model, as input into the structure factor, is refined against reflection data. New software, which can be integrated with standard single crystal data processing applications, was written to implement the above data reduction strategy.[35] To maintain compatibility with current data reduction programs, the software reads in a structure file in SHELX *.ins format and a reflection file in *.hkl format. Error minimization was performed as described above. Each set of atomic coordinates was refined separately, generating separate values of f' and f'' for each crystallographic site, which form the output of the program.

Reflection data from each of the eight wavelengths was input into the program with the structure file obtained from data collected at 0.41382×10^{-10} m. Values for f'' are strongly correlated with the overall structure factor (OSF) in the centrosymmetric case, preventing f'' from being a reliable source for data quantification. For that reason, f' values for the intersite and kagomé site are plotted in Figure 3. Beginning at a longer wavelength, the f' at the kagomé site goes through a sharp decline with the minimum at the Cu edge. The data increase until 1.29704×10^{-10} m, at which point they level off, maintaining linearity through the Zn edge. The absence of a

decline at the Zn edge indicates no population of Zn on the kagomé layer. Simulation of the calculated edge[36] provides an upper limit of 1% Zn on the kagomé layer (with an estimated total error, including experimental uncertainties, of $\sim$3%). At the intersite, beginning at a longer wavelength, the data decrease steadily, reaching a shallow minimum at the Cu edge. The data then increase, reaching a maximum and intersecting the f' data for the kagomé site at 1.3412×10^{-10} m; this is the point of equal real scattering amplitude for Cu and Zn. The data then decrease reaching a sharp minimum at the Zn edge and finally increase following the edge. Comparison of the intersite data to the calculated edges results in a best estimate of 15(2)% Cu on the intersite.

Confirmation of the above results proceeded through two well established methods of structural analysis. The radically different chemical environments on the kagomé plane and intersite suggested extended X-ray absorption fine structure (EXAFS) as a valuable technique for differentiating Cu from Zn, while the 30% difference in the neutron cross sections of Cu and Zn recommended the use of Rietveld refinement of NPD data. EXAFS data were collected on deuterated powder samples of $ZnCu_3(OH)_6Cl_2$ at the Cu and Zn K-edges. A Fourier transform of the Cu edge EXAFS data revealed a peak at 2.77 Å, corresponding to the Cu–Cl distance (Figure 4). The data at the Zn edge show no amplitude at a distance of 2.77 Å. Fits of the EXAFS data using FEFF showed the Zn occupancy on the kagomé lattice to be statistically insignificant from zero (Figure 3 inset), with additional parameters for mixing on the kagomé lattice leading to parameters with nonsensical values. Both data at the Zn edge and Cu edge reveal peaks at approximately 2 Å, which corresponds to the M–O bond distances. These peaks both manifest as weak contributions, particularly in the case of the Cu edge, where the peak is a shoulder on the Cu–Cl peak. The similar bond distances make quantitative assessment of Cu occupancy on the intersite challenging. These EXAFS results conclusively show no statistically significant Zn presence on the kagomé layer but cannot offer any quantitative information about the occupancy of Cu on the intersite layer.

(35) The program can be downloaded at http://occamy.chemistry.jhu.edu/anomalous.
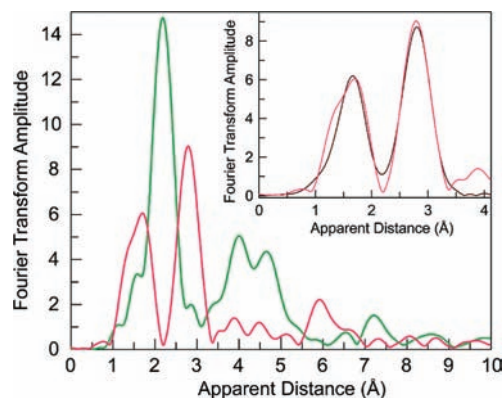
(36) Cromer, D. T.; Mann, J. B. *Acta Crystallogr.* **1968**, *A24*, 321–324.

Figure 4. Fourier transform of EXAFS data collected on a powder sample of $(Zn_{0.85}Cu_{0.15})Cu_3(OH)_6Cl_2$. Green and red lines represent data collected at the Cu and Zn K-edges respectively. Inset: FEFF fit of EXAFS data collected at the Zn edge from 0 to 4 Å; red and black lines represent the data and the fit, respectively. Two Zn sites were refined: the Zn intersite and Zn in the kagomé layer. The Zn intersite refined with a Zn−O distance of 2.09 Å with a coordination number of 6, while the kagomé site refined to a coordination number of zero, leading to a Zn occupancy on the kagomé layer which is statistically insignificant from zero.

Figure 5. Rietveld refinement of neutron powder diffraction data according to the formula $(Zn_{1-3x}Cu_{3x})Cu_3(OD)_6Cl_2$ which permits the intersite cation to vary in occupancy while holding the rest of the structure constant; x refines to 0.12. Inset: Comparison of the statistics of refining only the intersite cation (red triangles), refining only the kagomé cation (green circles), and refining both simultaneously while holding the ratio of Cu/Zn constant at 3:1 (black squares). The lines are the best fit.

Prior NPD measurements of $ZnCu_3(OH)_6Cl_2$ have contributed to the conclusion that there is significant Zn/Cu site mixing,[12,13] in which every Cu^{2+} removed from the kagomé plane is accounted for in the intersite, thus maintaining the formula of $ZnCu_3(OH)_6Cl_2$ obtained from ICP-AES. Rietveld refinement of previous NPD data led to a best fit for a compound with the formula $(Zn_{0.76}Cu_{0.24})(Cu_{0.91}Zn_{0.09})_3(OD)_6Cl_2$.[13] In order to allow for additional mixing scenarios, which might support both the EXAFS data and the new anomalous scattering results, and to determine the statistical significance of these formulas, NPD data were collected on a deuterated powder sample of herbertsmithite at beamline BT2 at NIST. The sample was synthesized as previously described[6] and determined to have Zn = 1 by powder X-ray diffraction (PXRD) and ICP-AES. Data were collected at 12 and 300 K to ensure no structural changes occurred at low temperature. Rietveld refinements were performed on the data obtained at 12 K, and the deuteration level was refined to 99(1)%. An initial refinement with the structural parameters of ordered herbertsmithite, $ZnCu_3(OD)_6Cl_2$, led to an $R(F^2)$ of 3.84. Three sets of refinements were performed on the data to evaluate the validity of site mixing. In the first refinement the composition of the intersite was held at Zn = 1, while the occupancy on the kagomé layer was modeled according to the formula $Zn(Cu_{1-x}Zn_x)_3(OD)_6Cl_2$, with values of $x = 0$ to $x = 0.20$ in intervals of 0.02. Refinement with these parameters did not lead to a statistically significant improvement in the data, with an average $R(F^2)$ of 3.74 and no clear minimum across the range of calculated x values. A similar refinement was then performed, holding the kagomé site at Cu = 3 and varying the intersite composition according to the formula $(Zn_{1-3x}Cu_{3x})Cu_3(OD)_6Cl_2$ (Figure 5). In this refinement, a gradual minimum of $R(F^2) = 3.625$ appears at $x = 0.12$. Finally, a refinement similar to literature precedent was performed.[13] In that refinement, the ratio of Zn/Cu was held at 1:3 as determined by ICP-AES. Both the kagomé layer and the intersite compositions were varied according to the formula $(Zn_{1-3x}Cu_{3x})(Cu_{1-x}Zn_x)_3(OH)_6Cl_2$. This refinement echoed the previously reported data, with a shallow minimum around $x = 0.10$ and $R(F^2) = 3.62$. However, when compared to the other refinement scenarios, it becomes obvious that adding mixing in the kagomé plane does not improve the statistics of the
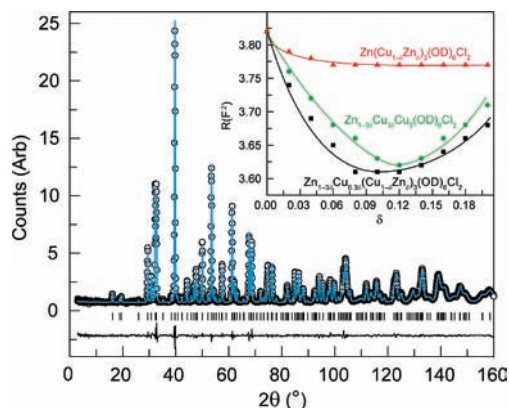
refinement compared to the model with no Zn mixing onto the kagomé plane, but mixing on the intersite, allowing the Zn/Cu ratio to deviate from 1:3 improves the fit. These data demonstrate that there is likely mixing on the intersite but the NPD data cannot resolve the question of mixing within the kagomé plane. Thus NPD data are also consistent with the result obtained from anomalous X-ray diffraction; i.e. there is Zn−Cu mixing on the intersite but only Cu on the kagomé site. We and others have assumed the end member of the $Zn_xCu_{4-x}(OH)_6Cl_2$ series to be "$x = 1$"; the anomalous scattering data presented here demonstrates that this is not the case and, owing to intersite mixing, the actual formula of the end-member compound is $(Zn_{0.85}Cu_{0.15})Cu_3(OH)_6Cl_2$. Notwithstanding, the fact that there is at most minimal Zn−Cu mixing within the kagomé layers implies that chemical disorder within the 2-D layers cannot be an explanation for the unusual magnetic properties observed.

Conclusion

X-ray anomalous scattering was used to determine the composition and degree of site mixing in the frustrated spin compound and RVB ground state candidate $Zn_xCu_{4-x}(OH)_6Cl_2$. The compound's composition of $(Zn_{0.85}Cu_{0.15})Cu_3(OH)_6Cl_2$ was verified by two alternate methods of structural characterization, establishing the validity of X-ray anomalous scattering as a structure characterization technique. The data effectively eliminate the possibility of Zn^{2+} impurities on the kagomé lattice, obviating chemical disorder in the kagomé layer as an explanation for the absence of magnetic order. These results are reminiscent of those found in the isomorphic compound $(Mg_{0.75}Cu_{0.25})Cu_3(OH)_6Cl_2$, in which the difference in electron count allows for assignment of metal occupancy through conventional crystallographic techniques.[8] In the case of the Mg analogue, no Mg is present on the kagomé plane, there is an upper limit of incorporation of Mg = 0.75 on the intersite, and only a faint magnetic transition remains. These results point toward some kind of unconventional electronic state. Recent low energy dynamic susceptibility measurements of $(Zn_{0.85}Cu_{0.15})Cu_3(OH)_6Cl_2$, which are in support of the conclusions drawn here, demonstrate a scaling relation similar to the case

for heavy-fermion metals,[37] potentially indicating that the ground state of herbertsmithite is a critical spin liquid.

The methodology presented here provides robust chemical information on the composition of crystallographic sites, even when the elements in question are very similar in scattering factor, and has wide-ranging potential applications beyond the $Zn_xCu_{4-x}(OH)_6Cl_2$ family. In chemistry, applications exist in the emerging fields of multimetallic metal−organic frameworks[38−40] and multimetallic small molecule catalysis.[41] Our new software integrates with standard protein crystallography software packages, providing another characterization method to identify the transition metal sites in heme and nonheme cofactors, an active area of research in structural biology.[42] Most

applications will be in materials science; for example, for the prototypical iron arsenide superconductor $LnO_{1-x}F_xFeAs$, this method makes it possible to distinguish oxygen from fluorine (which are virtually identical in both X-ray and neutron scattering factors) and settle once and for all the question of the actual formulas of the superconducting phase. We also envision its use in the study of many other strongly correlated materials in which the presence of chemical disorder may underlie the 'exotic' properties observed.

(37) Helton, J. S.; Matan, K.; Shores, M. P.; Nytko, E. A.; Bartlett, B. M.; Qiu, Y.; Nocera, D. G.; Lee, Y. S. *Phys. Rev. Lett.* **2010**, *104*, 147201/1–4.
(38) Dincă, M.; Long, J. R. *J. Am. Chem. Soc.* **2007**, *129*, 11172–11176.
(39) Corma, A.; Garca, H.; Llabrs, F. X.; Xamena, I. *Chem. Rev.* **2010**, *110*, 4606–4655.
(40) Botas, J. A.; Calleja, G.; Sánchez-Sánchez, M.; Orcajo, M. G. *Langmuir* **2010**, *26*, 5300–5303.
(41) Cook, T. R.; Esswein, A. J.; Nocera, D. G. *J. Am. Chem. Soc.* **2007**, *129*, 10094–10095.
(42) Balasubramanian, R.; Smith, S. M.; Rawat, S.; Yatsunyk, L. A.; Stemmler, T. L.; Rosenzweig, A. C. *Nature* **2010**, *465*, 115–119.